Title: SARS-CoV-2 induces acute neurological signs while Calcitonin Gene-Related Peptide (CGRP) signaling blockade reduces interleukin 6 (IL-6) release and weight loss in mouse models.

Abbreviated title: SARS-CoV-2 induces acute neurological signs while CGRP signaling blockade reduces interleukin 6 (IL-6) release and weight loss

Authors: Shafaqat.M. Rahman [1,co], David W. Buchholz[2,co], Brian Imbiakha.[2,co], Mason.C. Jager[3], Justin Leach, [1], Raven.M. Osborn [1], Ann O. Birmingham [1], Stephen Dewhurst[1], Hector C. Aguilar [2,*] , and Anne E. Luebke, [1,*]

Affiliations:

[1]University of Rochester Medical Center, Departments of Biomedical Engineering, Neuroscience, Microbiology and Immunology, Rochester, NY, USA;

[2] Cornell University, Department of Microbiology and Immunology, College of Veterinary Medicine, Ithaca, NY, USA.

[3] Cornell University, Department of Population Medicine, College of Veterinary Medicine, Ithaca, NY, USA.

[co] Contributed equally

*Send correspondence to: Anne E. Luebke (aluebke@ur.rochester.edu) or Hector C. Aguilar (haguilar@cornell.edu)

Submitting author: Anne E. Luebke (aluebke@ur.rochester.edu)

Number of Pages: 29

Number of Figures: 6

Number of Tables: 0

Number of words for Abstract: 151

Number of words for Significance Statement: 102

Number of words for Introduction: 591

Number of words for Discussion: 361

Conflict of interest statement: The authors declare no competing financial interests.

Acknowledgments: This research is supported by a COVID-19 research supplement to NIH R01 DC017261 (AEL). We would also like to thank Dr. Ralph S. Baric (UNC) for the MA-10 SARS CoV-2 virus stock, the BSL3 facility and staff in the Center for Advanced Research Technologies at the University of Rochester, and the ABSL3 facility and staff at Cornell University. We would also like to thank Shruti Aryal for assisting with data analysis.

Abstract:

COVID-19 can result in neurological symptoms such as fever, headache, dizziness, and nausea. We evaluated whether the Calcitonin Gene-Related Peptide (CGRP) receptor antagonist, olcegepant, used in migraine treatment could mitigate acute neuroinflammatory and neurological responses to SARS-COV-2 infection. We infected wildtype C57BL/6J and 129/SvEv mice, and a 129 αCGRP-null mouse line with a mouse-adapted SARS-CoV-2 virus, and evaluated the effect of CGRP receptor antagonism on the outcome of that infection. We determined that CGRP receptor antagonism provided protection from permanent weight loss in older (>12 m) C57BL/6J and 129 SvEv mice. We also observed acute fever and motion-induced dizziness in all older mice, regardless of treatment. However, in both wildtype mouse lines, CGRP antagonism reduced acute interleukin 6 (IL-6) levels by half, with virtually no IL-6 release in mice lacking αCGRP. These findings suggest that blockage of CGRP signaling protects against acute IL-6 release and subsequent inflammatory events after SARS-CoV-2 infection.

Significance Statement:

COVID-19 can cause neurological symptoms such as fever, headache, dizziness, and nausea. However, such neurological symptoms of SARS-CoV-2 infection have not been assessed in mouse models. Here, we infected two commonly used wildtype mice lines (C57BL/6 and 129S) with mouse-adapted SARS-CoV-2 – and demonstrated neurological signs that including motion-related dizziness. Further, we show that CGRP signaling blockade can reduce IL-6 release and reverse long-term weight loss associated with SARS-CoV-2 infection, without rescuing either fever and/or dizziness. These findings suggest that CGRP signaling blockade can be protective in acute SARS-CoV-2 infections, and raise the possibility that it may also impact long-term outcomes of infection.

Introduction

Coronavirus disease (COVID-19) caused by severe acute respiratory syndrome CoV-2 (SARS-CoV-2) has caused a 3-year, ongoing, world pandemic (Zhu et al. 2020). There is a sound premise supporting testing CGRP-receptor antagonists such as olcegepant as a way to mitigate the neuroimmune consequences of SARS-CoV-2 infection (Robertson 2020). While CGRP has pleotropic effects on the immune system, CGRP release occurs as a result of SARS-CoV-2 activation of the transient receptor potential (TRP) channels; and is implicated in COVID-19 neurological symptoms such as fever, headache, dizziness, nausea pain, and the subsequent release of interleukin 6 (IL-6) (Assas, Miyan, and Pennock 2014; Assas, Pennock, and Miyan 2014; Channappanavar and Perlman 2017). IL-6 is an important mediator of inflammation that is often elevated in severe COVID-19 infection, and may be involved in the hyperimmune response cascade (cytokine storm) and the polarization of T-cell responses (Aghagoli et al. 2021; Liu et al. 2020). Headache, nausea, and dizziness are common neurological manifestations of COVID-19 infection (Bohn et al. 2020; Saniasiaya and Kulasegarah 2021; Doyle 2022), and in COVID-19 patients headache severity has been correlated with IL-6 levels (Bolay et al. 2021; Karadas et al. 2021). However, there have been no studies on animal models investigating dizziness and fever after SARS-CoV-2 infection (Carpenter, Yang, and Xu 2023) .

Studies have shown that both SARS-CoV-1 (2002 outbreak) and SARS-CoV-2 (2019 outbreak) enter the body by binding to the angiotensin-converting enzyme 2 (ACE2) cell receptor (Kuba et al. 2005; Ziegler et al. 2020). However, due to sequence and structural differences between mouse ACE2 and human ACE2, human SARS coronaviruses exhibit a species-restricted tropism and are inefficient at infecting wild-type mice. To overcome this obstacle, the Baric laboratory modified the clinical SARS-CoV-2/USA-WA1 variant to gain the ability to bind to the murine ACE2 receptor after serial passaging in mice, to generate the MA10-SARS-CoV-2 virus (Dinnon et al. 2020, 2021); we used this mouse-adapted virus in most of our study.

We first assessed both neurological symptoms of fever and dizziness/nausea in mouse models after infection with the MA10-SARS-CoV-2 virus. As a readout of the nausea-like state present after SARS-CoV-2 infection, we examined hypothermic responses to provocative motion, as we have previously used to assess migraine nausea pain (Biorxiv doi.org/10.1101/2022.06.03.494762) and others have used to assess motion-sensitivity in transgenic mouse models (Tu et al. 2017). Studies have demonstrated that provocative motion causes robust and prominent hypothermic responses in rats, humans, house musk shrews, and mice. These decreases in body temperature can represent a biomarker of a nausea-like state in laboratory animals as: i) temperature changes are provoked both by motion and by chemical emetic stimuli, ii) differential pharmacological sensitivity of these responses mirrors sensitivity in humans, iii) motion-induced hypothermia *precedes* emetic (vomiting) episodes, and iv) there is a clear parallel in hypothermic responses between animals and humans in underlying physiological mechanism - cutaneous vasodilatation that favors heat loss (Del Vecchio et al. 2014; Mazloumi Gavgani, Hodgson, and Nalivaiko 2017; Ngampramuan et al. 2014; Romano et al. 2017; Tu et al. 2017). In the nausea/dizziness assay after provocative motion there is a decrease in head temperature and an increase in tail temperature. We have shown that in wildtype C57BL/6Jmice injection of Calcitonin Gene-Related Peptide (CGRP) prolongs this head temperature response and blunts the transient tail temperature increase, whereas a CGRP-receptor antagonist can reverse these CGRP-induced changes (Doods et al. 2000; Mallee et al. 2002) and Biorxiv doi.org/10.1101/2022.06.03.494762. Therefore, we investigated if a MA10-SARS-CoV-2 viral infection would show similar acute dizziness/nausea responses as CGRP injection, and if antagonizing CGRP signaling could reduce these dizziness/nausea responses.

116 **Materials and Methods**

117 **Animals**

118 A total of 180 mice (120 M/60F) were used in these studies, either 129SvEv (Taconic
119 129SVE) or C57B6/J (JAX 0664) or αCGRP (-/-) null mice on a 129SvEv background. Prior to
120 SARS-CoV-2 infection, mice were bred and housed under a 12 to 12 day/night cycle at the
121 University of Rochester 's Vivarium under the care of the University of Rochester's Veterinary
122 Services personnel. Mice were implanted with transponder chips (Backagin Microchip FDX-B
123 ISO 11784/11785) to allow for blinded identification; and when relevant, implanted with pellets
124 containing placebo or olcegepant (BIBN4096, Tocris; 2 mg/kg/day/SQ; Innovative Research of
125 America, Inc.). After pretesting was performed, mice were transferred to Cornell's ABSL3
126 facility, and acclimated prior to virus infection and testing. All animal procedures were approved
127 both by the University of Rochester's and Cornell University's IACUC committees and
128 performed in accordance with NIH standards.

129

130 **Virus propagation**

131 Vero-E6 cells (obtained through BEI resources, NIAID, NIH, NR-53726) were cultured in
132 Eagle's Minimum Essential Medium (ATCC, #30-2003) supplemented with 10% (vol/vol) fetal
133 bovine serum (FBS) (Gibco, CA) and 1% penicillin-streptomycin (Pen-Strep, Life Technologies)
134 at 37°C in a 5% (vol/vol) CO_2 atmosphere. Viral stocks of mouse-adapted SARS-CoV-2 (MA10)
135 (obtained from the laboratory Dr. Ralph Baric) were propagated in Vero-E6 cells in 2% (vol/vol)
136 FBS and 1% penicillin-streptomycin at 37°C at a multiplicity of infection (MOI) of 0.1. Viral stock
137 titers were determined by $TCID_{50}$ analysis. Viral propagation involving live SARS-CoV-2 was
138 conducted in Biosafety level 3 (BSL3) facilities both at the University of Rochester and at
139 Cornell University.

140

141 **Animal Biosafety level 3 (ABSL3) facility and viral inoculations**

142 Mice were anesthetized using isoflurane and subsequently intranasally infected with MA-
143 10 SARS-CoV-2. For infection with live virus, drops of the pre-characterized viral stock were
144 administered into the rostral meatus of the nose, with a total volume of 50 µL per mouse. Daily
145 monitoring and weighing of the mice were conducted until they reached a predetermined
146 humane endpoint of 20% weight loss from their starting weight and/or severe clinical signs, at
147 which point animals were humanely euthanized. Mouse studies were conducted in a BSL-3
148 laboratory and in accordance with protocols approved by the Institutional Animal Care and Use
149 Committee at Cornell University (IACUC mouse protocol # 2017-0108 and BSL3 IBC # MUA-
150 16371-1). See Fig. 1A.

151

152 **Motion-Induced Thermoregulation Testing**

153 Tu et al. first noticed thermoregulatory changes in the temperatures of the heads,
154 bodies, and tails of mice, in response to provocative motion (Tu et al. 2017) . We therefore
155 adapted their protocol for the present study (Biorxiv doi.org/10.1101/2022.06.03.494762).
156 Head and tail temperatures of C57B6/J mice were measured for a total of 45 minutes using a
157 FLIR E60 IR camera (model: E64501), as depicted in Fig. 1A. This camera was connected to a
158 tripod and positioned approximately 43 cm above an open, plexiglass box (mouse box) used to
159 house an individual mouse during testing. Both the tripod and mouse box were securely
160 attached to the shaker's base. Briefly, baseline measurements were recorded for five minutes
161 prior to the provocative motion (-5 to 0 mins). The provocative motion was an orbital rotation (75
162 rpm, 2-cm orbital displacement), and mice were video-recorded for 20 minutes (0 to 20 mins).
163 After 20 minutes, the provocative motion was turned off, and mice were video-recorded for an
164 additional 20 minutes to measure recovery to baseline (20 to 40 mins) as schematized in Figs.
165 1A and 2. Head and tail temperatures were measured after data retrieval using the software
166 FLIR Tools+. Tail and head temperatures were measured within predefined field of views:

167 square region (3x3 mm) for tail, and circular region (10x10 mm) for head. Tail measurements
168 occurred 2 cm from the base of the tail and head measurements occurred at the center of the
169 head image, in between the mouse's ears. Infrared imaging data was collected every minute
170 during baseline measurements, and every 2 minutes during and after the provocative motion.
171 We quantified thermoregulatory changes to provocative motion by comparing changes in tail
172 vasodilatations, and we approximated the magnitude of the head hypothermia based on second
173 order curve fit estimates. Transient increases in the tail temperature of the mouse to provocative
174 motion are referred to as Δ *tail vasodilatations* (^{o}C), and were computed by subtracting the tail
175 temperature at time t = 0 minutes (rotation ON) from the max tail temperature measured during
176 the first 10 mins of the rotation ($0 \leq t \leq 10$).

177

178 **Pulse Oximetry**

179 A mouse Stat Jr X (Kent Scientific) was used to measure oxygen saturation (O2%) of
180 mice (see Fig. 1B). The O_2 sensor was applied to the rear leg, and data were recorded following
181 readout stabilization, defined as an unchanging recording over 5 seconds.

182

183 **BAL harvest and tissue processing**

184 Mice were euthanized with CO_2 , and bronco-alveolar lavage BAL fluid was removed
185 from the lung; animals then underwent laparotomy and sternotomy with subsequent left and
186 right ventricular cardiac perfusion with 20 mL total of PBS. Lungs were treated with 4%
187 paraformaldehyde/PBS (volume/volume) for a minimum of 72 hours to ensure full viral
188 inactivation. Tissues were taken out of the BSL3 facility and underwent dehydration with ethanol
189 and were later embedded in paraffin blocks for histological analysis.

190

191 **Histopathology**

192 For histological examination, mouse lungs were collected directly after euthanasia and
193 placed in 10% neutral buffered formalin for 72 h, after which tissues were embedded in paraffin.
194 Four-micrometer tissue sections were stained with hematoxylin for analysis.
195 Immunohistochemistry and digital image analysis for SARS-CoV-2 nucleocapsid was performed
196 as previously described (Shapira et al. 2022). Briefly, 4 μm tissue sections were labeled with a
197 rabbit IgG monoclonal antibody against SARS-CoV-2 nucleocapsid protein (GeneTex;
198 GTX635679) at a 1:5,000 dilution and processed using a Leica Bond Max automated IHC
199 Stainer. Digital image analysis was performed using QuPath software v.0.2.3 (Achanta et al.
200 2012; Bankhead et al. 2017; Shapira et al. 2022; Shapira et al. 2021).

201

202 **Imaging**

203 Histological specimens were visualized using a Zeiss Axioplan 2 microscope.
204 Immunohistochemistry (IHC) and hematoxylin and eosin (HE) stained slides for each specimen
205 were photographed in sequential order. In Adobe Photoshop, all images were sized with a
206 2080x2080 pixel frame and cropped to a uniform resolution of 1500x1500 pixels. IHC images
207 were further analyzed using Color Selection and Magic Wand tools where areas containing
208 brown staining were manually selected and cut into a separate layer. All images were exported
209 into JPEG format. For staining percentages, quantification was performed using ImageJ.
210 Images were converted from RGB Color into 8-bit grayscale and made Binary to set an
211 automated threshold. Area was then calculated with the Analyze Particles function. Circularity of
212 staining was assessed using the Circularity parameter set to 0.9-1.0.

213 **Quantification of lavage cytokines by ELISA**

214 Immulux 4HBx plates (ThermoFisher Scientific, #3855) were coated with IL-6 capture
215 antibody (ThermoFisher Scientific, MP5-20F3) and left overnight at 4°C. Wells were washed five

216 times with PBS+0.05% Tween 20 and blocked with PBS+5% dry milk solution (Bio-Rad,
217 1706404) for 1 hour at room temperature. 50µL of lavage sample or standard (R&D systems,
218 406-ML-005/CF) was added to the blocked wells for 2 hours at room temperature. Bound
219 cytokine was detected using a biotinylated IL-6 detection antibody (ThermoFisher Scientific,
220 MP5-32C11), streptavidin horseradish peroxidase (strep-HRP), and tetramethylbenzidine (TMB)
221 (ThermoFisher Scientific, 34028). Wells were washed three times following the addition of
222 detection antibody and strep-HRP. Reactions were stopped with 2N H_2SO_4 and ODs were read
223 at 450nm. Cytokine concentrations for each sample were determined by plotting OD values on a
224 standard curve using IL-6 recombinant protein. All testing was performed in triplicate.

225

226 **Statistics**

227 Two-way mixed effects (ME) models were used to assess % weight loss, and core
228 temperatures (^{o}C) across the factors: i) placebo vs olcegepant protection and ii) dpi. Two-way
229 ME models were also used to assess: i) viral infection vs pretest and ii) placebo vs olcegepant
230 protection for tail vasodilation responses at 3 dpi. Bonferroni multiple comparisons test was the
231 preferred post-hoc analysis method. X-intercept analyses of head recovery (mins) were
232 conducted assuming a quadratic model, least squares regression fitting, and constraints where
233 the x-intercept must be greater than x = 20 mins and the curve fit was approximated to x = 50
234 mins. Nested 1-way ANOVAs with Tukey post hoc was used to analyze BAL IL-6
235 concentrations and H&E staining (positive SARS-CoV-2 cells per mm^2).

236

237

238 **Results**

239 **MA-10 SARS-CoV-2 infection induces a fever-like state and disrupts**
240 **thermoregulation to provocative motion.** We measured baseline head temperatures in 18
241 month-old male /6J, 129SvEv, and 129 αCGRP-null groups of mice during pretesting and 3

242 days post-infection (dpi) with 10^5 pfu of MA-10 SARS-CoV-2 virus (**Fig. 2A&B**). Our results
243 showed a higher head temperature at 3 dpi, indicating a fever in all mice, regardless of strain
244 and olcegepant pretreatment (**Fig. 2B**).

245 We also measured motion-induced thermoregulation and weight changes in 18 month-
246 old male C57BL/6J, 129SvEv, and 129 αCGRP-null groups of mice at 3 dpi with 10^5 pfu of MA-
247 10 SARS-CoV-2 virus (**Fig. 3A**). Motion-induced thermoregulation was pre-tested in each
248 mouse 5-7 days prior to the infection. During the pre-test, we observed transient tail vasodilation
249 in response to provocative, nauseating stimuli (**Fig 3B,C,D**). The assay involved a 5-minute
250 baseline recording, a 20-minute rotation period (75 rpm, 1 cm orbital displacement), and a 20-
251 minute recovery period (as shown in **Figs. 1B and 3A**). Tail temperature profiles also indicated
252 a fever-like state after infection with MA-10 SARS-CoV-2, with higher tail temperatures at all
253 time points during the 3 dpi test than during the pretest (**Fig. 3B,C,D**). We computed a shift in
254 the Δ tail vasodilations by subtracting the magnitude of Δ tail vasodilations at 3 dpi from an
255 animal's pretest Δ tail vasodilation. With the exception of infected αCGRP-null mice, we
256 observed a decrease in the magnitude of tail vasodilations in infected mice compared to their
257 pretest, as indicated by a negative change in the Δ tail vasodilation - which is a sign of less
258 severe dizziness.

259 Typically, a twenty-minute provocative rotation in mice causes observable hypothermia,
260 and an additional 20-minute recovery period is needed for the mice to recover to their baseline
261 head temperature. Interestingly, we observed that viral infection delayed this recovery period, as
262 seen in our raw data (**Fig. 3 E,F,G**). Using a second-order polynomial fit ($B_0 + B_1X + B_2X^2$), we
263 estimated the time required for the mice to recover back to their baseline head temperature by
264 interpolating a curve fit to t = 50 minutes (**Fig. 3H).** We then computed a Δ head recovery by
265 subtracting the recovery period at 3 dpi from the pretest, where a positive Δ head recovery
266 indicated a longer recovery period due to the infection. In all infected males, regardless of
267 olcegepant treatment or strain, we observed a longer recovery period at 3 dpi ($p < 0.0001$). No

268 protective effects were seen by olcegepant in head temperature recovery for either strain (**Fig.**
269 **3H**).

270

271 **Olcegepant blockage or developmental loss of CGRP receptor leads to reduced IL-6**
272 **production in response to MA-10 infection**

273 SARS-CoV-2 infected 129/SvEv mice treated with olcegepant pellets had lower
274 interleukin 6 (IL-6) concentrations in their bronchoalveolar lavage (BAL) as compared to mice
275 treated with placebo (**Fig. 4B**). Congruently, the lower IL-6 concentrations in olcegepant-treated
276 mice were similar to the IL-6 concentrations measured in the αCGRP-null (-/-) mice (**Fig 4B**),
277 which is consistent with the relationship between CGRP and IL-6 levels in migraines (Han
278 2019). In C57BL/6J mice, similar observations regarding olcegepant's effects in reducing IL-6
279 post-infection were observed but did not reach statistical significance (**Fig 4A**).

280 **Older mice treated with olcegepant recovered from the initial weight loss by 7 dpi.**

281 When 18-month-old C57 or 129S mice were infected with MA-10, those pretreated with
282 olcegepant pellets showed a faster recovery to baseline weight compared to mice that received
283 placebo pellets. This effect was observed in both female and male C57BL/6J mice (**Fig. 5A**), as
284 well as in older female and male 129SvEv mice (**Fig. 5B**). Notably, 129S αCGRP (-/-) null mice
285 of either sex experienced similar trends as 129S WT mice given olcegepant (**Fig. 5E**). Older
286 infected mice exhibited lower core temperatures compared to the uninfected groups; however,
287 olcegepant had no distinguishable effect on core temperatures regardless of age or strain (**Fig.**
288 **5 B,D,F**). In addition, MA-10 infection did not significantly impact O_2% saturation in mice
289 regardless of age, sex, or strain. However αCGRP-null mice exhibited lower weight loss trends
290 following virus infection that did WT mice - suggesting that the αCGRP-null mice have a
291 reduced sensitivity to the MA-10 virus.

292 Histological analysis of lung tissue revealed no significant differences in the number of
293 SARS-CoV-2 infected cells in the lungs of C57BL/6J or 129S WT mice at 3 dpi (**Fig. 6 A&B**).
294 However, olcegepant-protected mice and αCGRP-null mice showed reduced staining for SARS-
295 CoV-2 when compared to placebo-treated mice, and this observation correlated with IL-6 levels.
296 **Fig. 6 C&D** shows SARS-CoV-2 staining (scale = 100 μm) of C57BL/6J (**C**) and 129S (**D**) lung
297 tissues.

298

299

300 **Discussion:**

301 Early in the pandemic, there was a controversy as to whether CGRP plasma levels were
302 increased or decreased in COVID-19 disease (Abobaker and Darrat 2021; Ochoa-Callejero et
303 al. 2021). However, a recent study with a relatively greater number of patients showed that
304 elevated CGRP plasma levels are correlated with increased disease severity in hospitalized
305 COVID-19 patients (Rizzi et al. 2022). In our study, the migraine drug olcegepant (small
306 molecule CGRP receptor antagonist) reduced IL-6 release at three days post-infection (3 dpi) in
307 two distinct wildtype mouse strains (C57B6 and 129S). Interestingly however, there was not a
308 similar protective effect on fever or on the dizziness/nausea-like state elicited by SARS-CoV-2
309 MA-10 in these same infected mice, as tested at 3 dpi. However, we did replicate in the mouse
310 model both the fever and vestibular symptoms observed in COVID patients (Aedo-Sanchez,
311 Gutierrez, and Aguilar-Vidal 2023; Jeong et al. 2021).

312 A few studies have investigated CGRP antagonism on individuals infected with SARS-
313 CoV-2. In one study (Caronna et al. 2021), no deleterious effects of CGRP antagonism were
314 found, and no differences in symptom severity were found between CGRP antagonism to other
315 treatment modalities in migraine subjects. However, in this study, patients were not stratified by
316 age. We observed CGRP antagonism was protective from weight loss and IL-6 release only in
317 older mice. COVID-19 symptoms are more severe and mortality rates are higher in aged
318 human patients, adding significance to our results. Further, two relatively recent case studies
319 showed that increased headaches after SARS-CoV-2 infection can be treated with CGRP
320 monoclonal antibodies (Grassini et al. 2021; Ozkan et al. 2022). Our study suggests that
321 olcegepant or other CGRP treatments may be further explored particularly to treat headaches or
322 migraines in aged individuals and/or those with high IL-6 levels upon COVID-19 infection.

323 In conclusion, in addition to the acute effects studied here, antagonizing CGRP signaling
324 may be therapeutic against long COVID, as long COVID patients also show higher IL-6 plasma
325 levels (Littlefield et al. 2022). As long COVID has been demonstrated in mouse models (Dinnon

326 et al. 2022), future plans include investigating if antagonizing CGRP signaling in preclinical

327 models can mitigate associated neurological symptoms of long COVID.

328

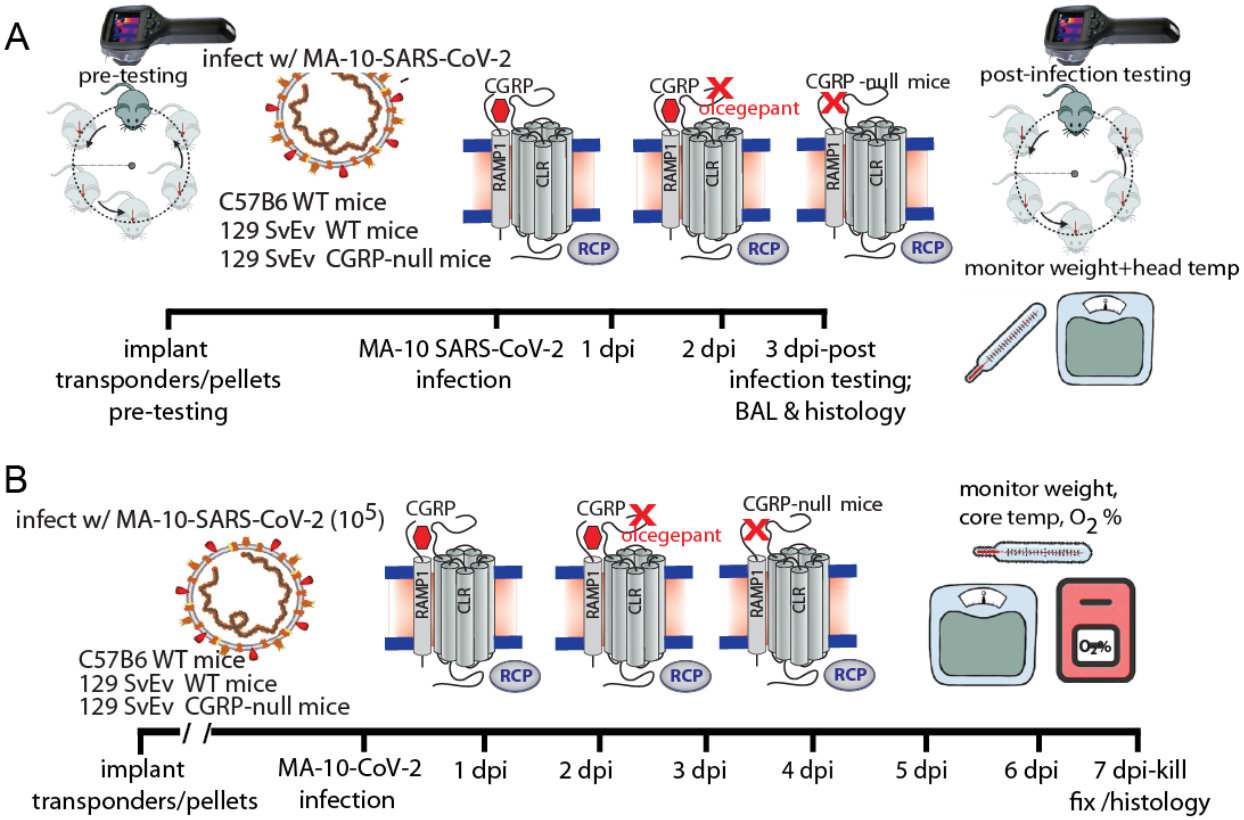
A
pre-testing
infect w/ MA-10-SARS-CoV-2
C57B6 WT mice
129 SvEv WT mice
129 SvEv CGRP-null mice
CGRP
RAMP1
CLR
RCP
olcegepant
CGRP -null mice
post-infection testing
monitor weight+head temp
implant transponders/pellets pre-testing
MA-10 SARS-CoV-2 infection
1 dpi
2 dpi
3 dpi-post infection testing; BAL & histology
B
infect w/ MA-10-SARS-CoV-2 (10^5)
C57B6 WT mice
129 SvEv WT mice
129 SvEv CGRP-null mice
CGRP-null mice
monitor weight, core temp, O2 %
implant transponders/pellets
MA-10-CoV-2 infection
1 dpi
2 dpi
3 dpi
4 dpi
5 dpi
6 dpi
7 dpi-kill fix /histology

Fig. 1

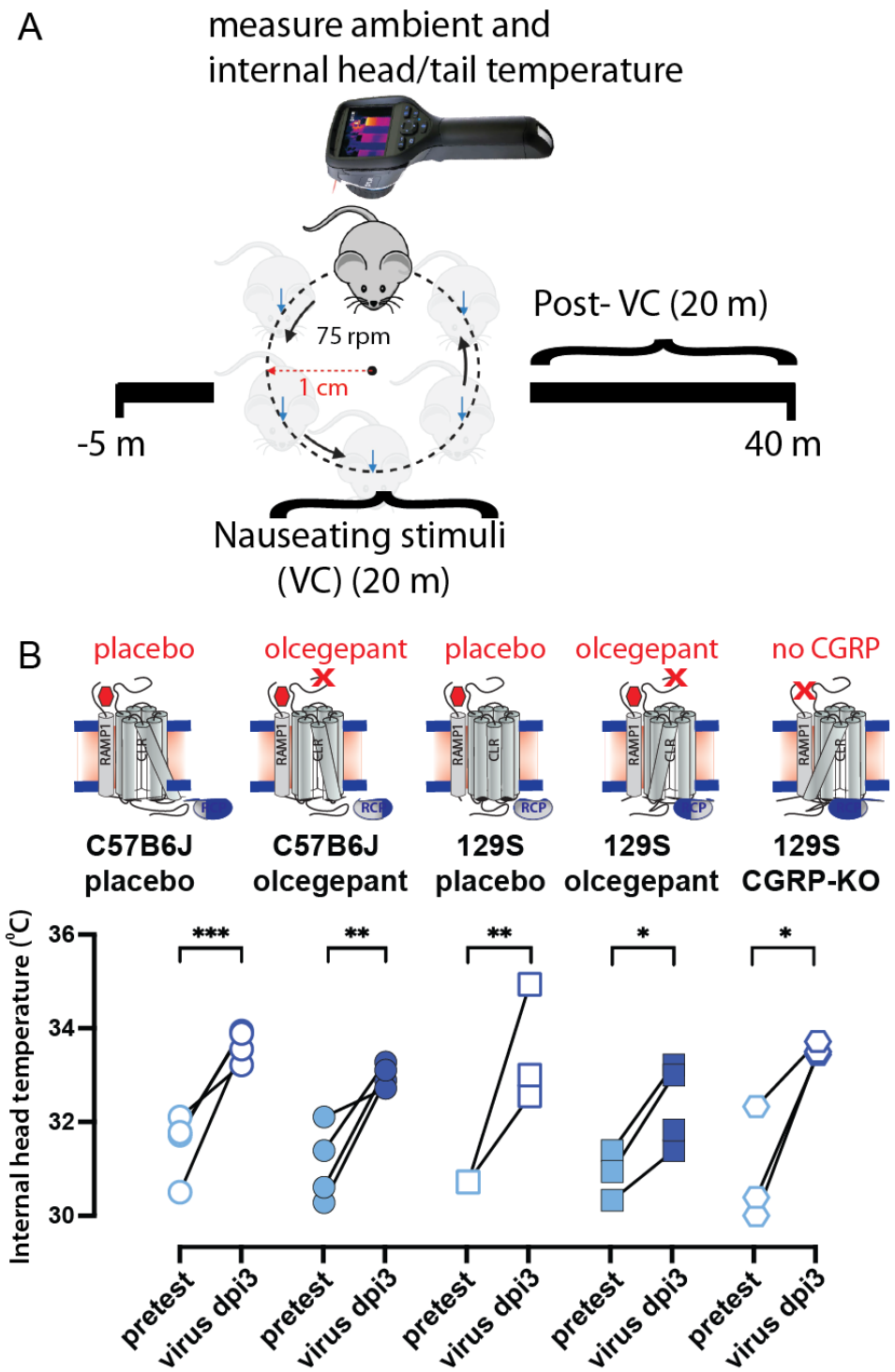
A
measure ambient and
internal head/tail temperature
75 rpm
1 cm
-5 m
Post- VC (20 m)
40 m
Nauseating stimuli
(VC) (20 m)
B
placebo
olcegepant
placebo
olcegepant
no CGRP
RAMP1
CLR
RCP
C57B6J
placebo
C57B6J
olcegepant
129S
placebo
129S
olcegepant
129S
CGRP-KO
Internal head temperature (°C)
36
34
32
30
***
**
**
*
*
pretest
virus dpi3

Fig. 2

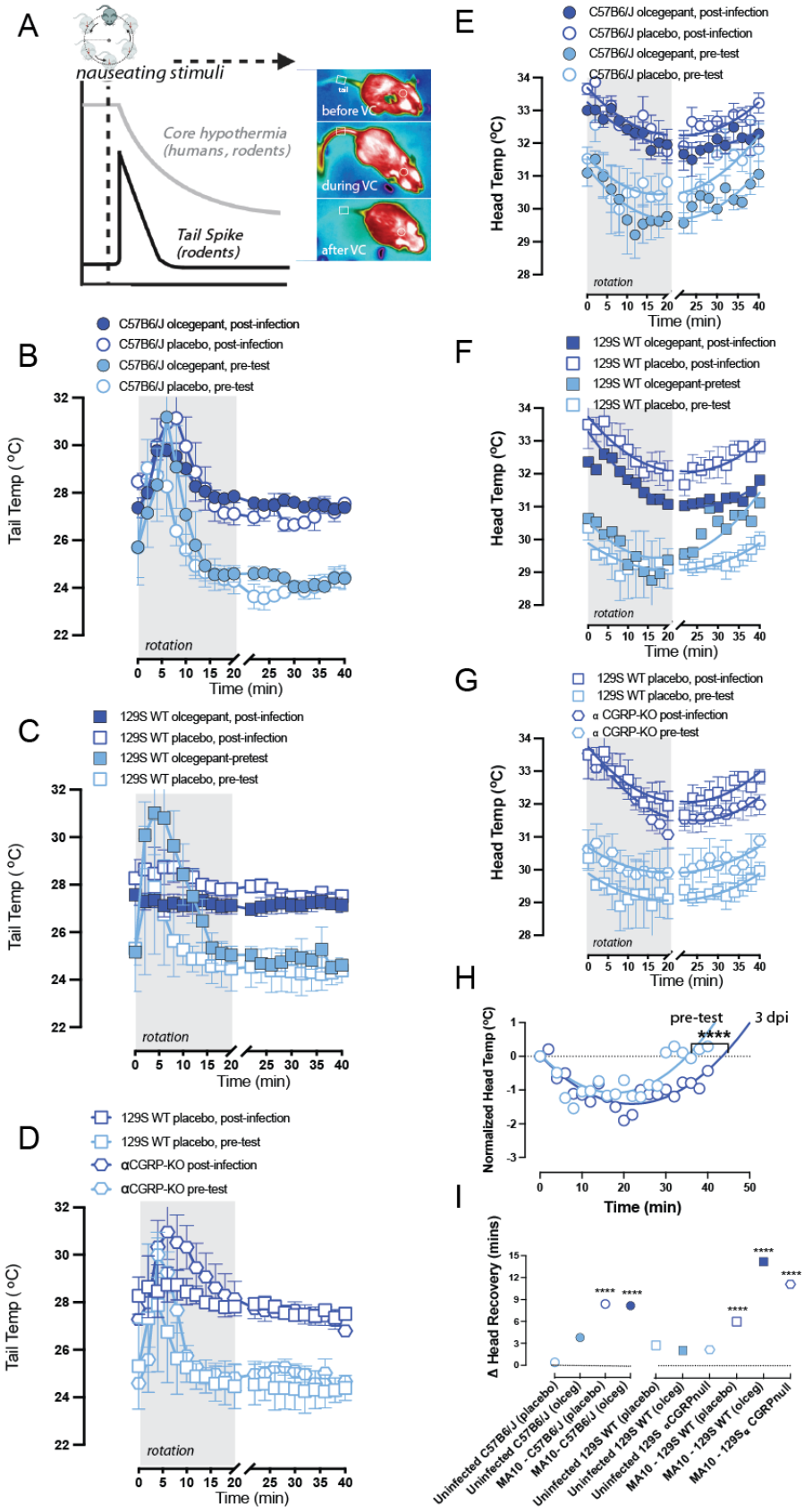
A
nauseating stimuli
Core hypothermia
(humans, rodents)
Tail Spike
(rodents)
before VC
during VC
after VC
B
C57B6/J olcegepant, post-infection
C57B6/J placebo, post-infection
C57B6/J olcegepant, pre-test
C57B6/J placebo, pre-test
Tail Temp (°C)
rotation
Time (min)
C
129S WT olcegepant, post-infection
129S WT placebo, post-infection
129S WT olcegepant-pretest
129S WT placebo, pre-test
Tail Temp (°C)
rotation
Time (min)
D
129S WT placebo, post-infection
129S WT placebo, pre-test
αCGRP-KO post-infection
αCGRP-KO pre-test
Tail Temp (°C)
rotation
Time (min)
E
C57B6/J olcegepant, post-infection
C57B6/J placebo, post-infection
C57B6/J olcegepant, pre-test
C57B6/J placebo, pre-test
Head Temp (°C)
rotation
Time (min)
F
129S WT olcegepant, post-infection
129S WT placebo, post-infection
129S WT olcegepant-pretest
129S WT placebo, pre-test
Head Temp (°C)
rotation
Time (min)
G
129S WT placebo, post-infection
129S WT placebo, pre-test
α CGRP-KO post-infection
α CGRP-KO pre-test
Head Temp (°C)
rotation
Time (min)
H
pre-test
3 dpi
****
Normalized Head Temp (°C)
Time (min)
I
Δ Head Recovery (mins)
Uninfected C57B6/J (placebo)
Uninfected C57B6/J (olceg)
MA10 - C57B6/J (placebo)
MA10- C57B6/J (olceg)
Uninfected 129S WT (placebo)
Uninfected 129S WT (olceg)
Uninfected 129S αCGRPnull
MA10 - 129S WT (placebo)
MA10 - 129S WT (olceg)
MA10 - 129Sα CGRPnull

Fig. 3

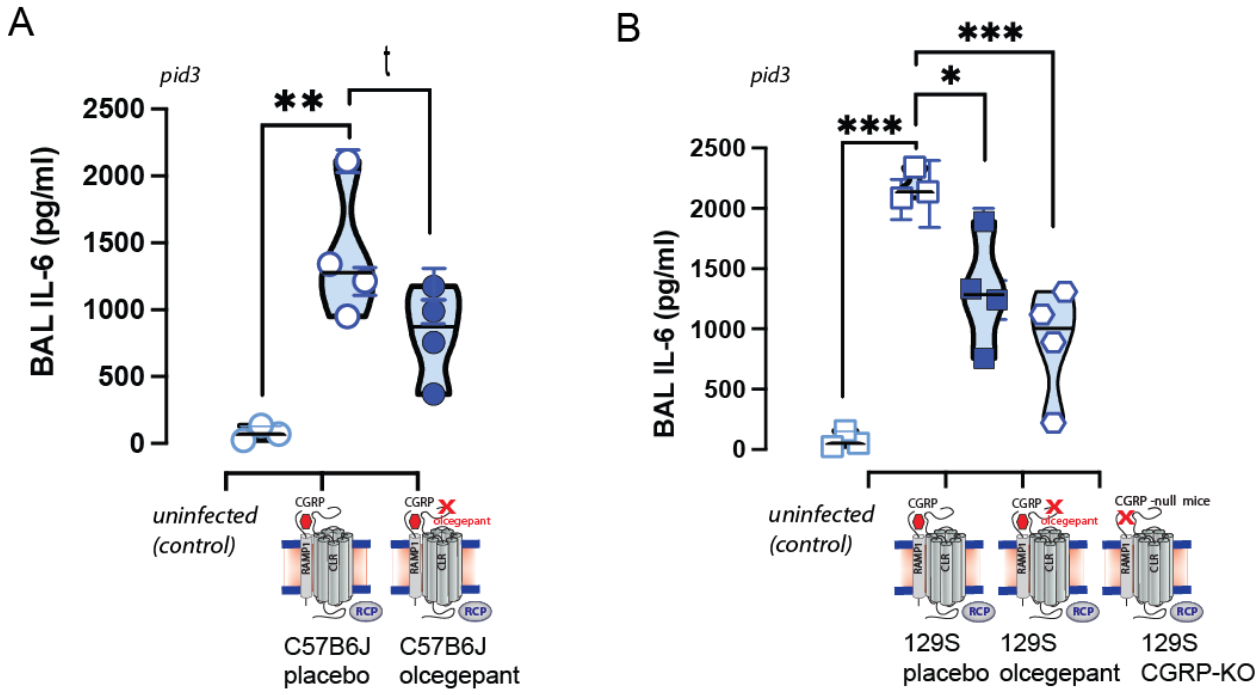

339

340

341 Fig. 4

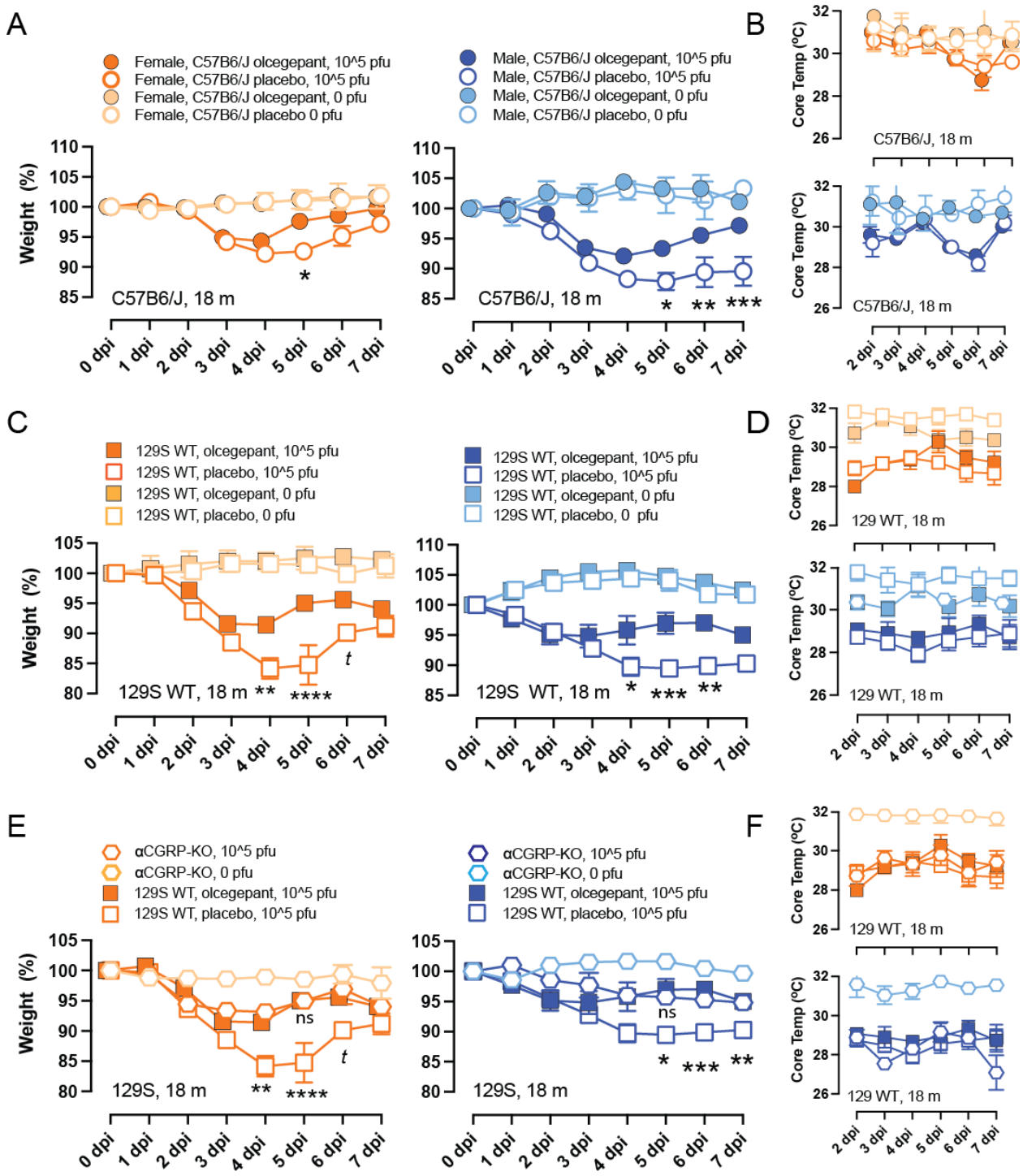
A
Female, C57B6/J olcegepant, 10^5 pfu
Female, C57B6/J placebo, 10^5 pfu
Female, C57B6/J olcegepant, 0 pfu
Female, C57B6/J placebo 0 pfu
Male, C57B6/J olcegepant, 10^5 pfu
Male, C57B6/J placebo, 10^5 pfu
Male, C57B6/J olcegepant, 0 pfu
Male, C57B6/J placebo, 0 pfu
Weight (%)
C57B6/J, 18 m
B
Core Temp (°C)
C57B6/J, 18 m
C
129S WT, olcegepant, 10^5 pfu
129S WT, placebo, 10^5 pfu
129S WT, olcegepant, 0 pfu
129S WT, placebo, 0 pfu
129S WT, 18 m
D
129 WT, 18 m
E
αCGRP-KO, 10^5 pfu
αCGRP-KO, 0 pfu
129S WT, olcegepant, 10^5 pfu
129S WT, placebo, 10^5 pfu
129S, 18 m
ns
F
0 dpi
1 dpi
2 dpi
3 dpi
4 dpi
5 dpi
6 dpi
7 dpi

Fig. 5

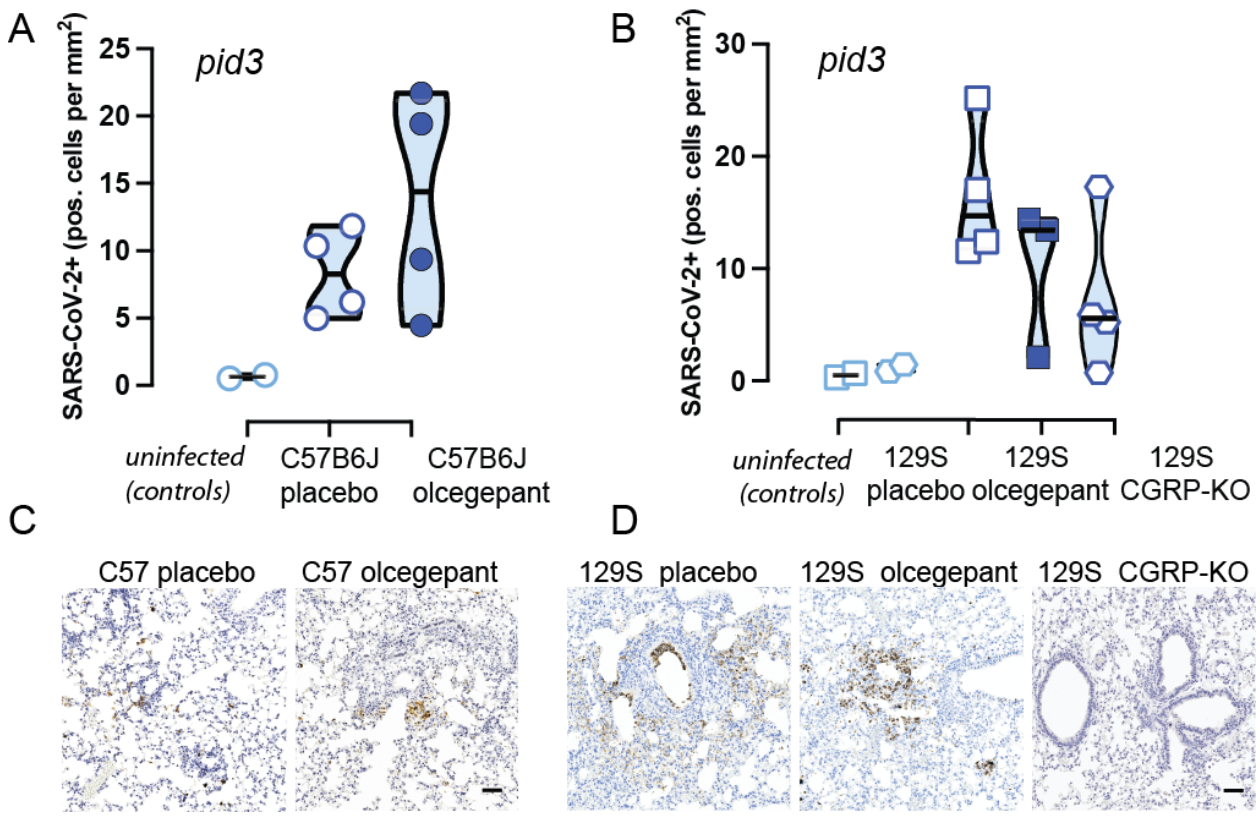
A
pid3
SARS-CoV-2+ (pos. cells per mm²)
25
20
15
10
5
0
uninfected (controls)
C57B6J placebo
C57B6J olcegepant
B
pid3
SARS-CoV-2+ (pos. cells per mm²)
30
20
10
0
uninfected (controls)
129S placebo
129S olcegepant
129S CGRP-KO
C
C57 placebo
C57 olcegepant
D
129S placebo
129S olcegepant
129S CGRP-KO

Fig. 6

364 **Figure Legends:**

365 **Fig. 1.** The study timelines are depicted. **A.** WT mice were infected with 10^5 pfu of MA-10
366 SARS-CoV-2 in the presence of placebo or CGRP-receptor antagonist olcegepant slow-release
367 pellets (olcegepant, BIBN4096, Tocris; 2 mg/kg/day/SQ) or mice lacking CGRP were infected
368 with the same virus; animals were then assessed for motion-induced nausea (dizziness) at 3
369 days after viral infection (dpi). At the completion of the nausea testing at 3dpi, bronchoalveolar
370 lavage (BAL) samples were collected for ELISA and lung tissue was obtained from control and
371 virus-infected animals at 3 dpi. Nausea (dizziness) was assessed for 45 minutes when mouse
372 was subjected to an orbital motion, noting temperature profiles (head and tail). **B.** WT mice
373 were infected with 10^5 pfu of MA-10 SARS-CoV-2 in the presence of placebo or CGRP-receptor
374 antagonist olcegepant slow-release pellets (olcegepant, BIBN4096, Tocris; 2 mg/kg/day/SQ) or
375 mice lacking CGRP were infected with the same virus; animals were then monitored for
376 changed in weight, core temperature and oxygen (O_2) saturation from 0 to 7 dpi.

377

378 **Fig. 2.** As shown in the **Fig 1A** timeline, older C57B/6, 129SvEv, and 129 mice lacking CGRP
379 were assessed for nausea (dizziness) when subjected to an orbital rotation, noting temperature
380 profiles (head and tail). **A.** Head and tail temperatures of mice were measured for a total 45
381 minutes using a FLIR E60 IR camera (model: E64501). This camera was connected to a tripod
382 and positioned approximately 43 cm above an open, plexiglass box (mouse box) used to house
383 an individual mouse during testing. Both the tripod and mouse box are securely attached to the
384 shaker's base. Briefly, baseline measurements were recorded for five minutes prior to the
385 provocative motion (-5 to 0 mins). The provocative motion was an orbital rotation (75 rpm, 2-cm
386 orbital displacement), and mice were recorded for 20 minutes (0 to 20 mins). After 20 minutes,
387 the provocative motion was turned off, and mice were recorded for an additional 20 minutes to
388 measure recovery to baseline (20 to 40 mins). Three mouse strains were tested: C57/B6J WT,
389 129S WT, and 129S αCGRP-null mice. Within each wild type (WT) strain, four groups of mice

390 were tested: placebo only, olcegepant only, placebo with 10^5 MA-SARS-CoV-2, and olcegepant
391 with 10^5 SARS-CoV-2 MA-10. Virus-infected mice were tested at Cornell University's ABSL-3
392 environment, with all pre-infection testing performed at University of Rochester. **B.** All tested
393 mice experienced a fever-like state 3 days post-viral infection (3 dpi). Olcegepant did not have a
394 protective effect in reducing this acute fever-like state at 3 dpi.

395

396 **Fig. 3. A.** Upon provocative motion, humans and mice will show a drop in head temperature
397 that recovers once rotation is ceased, and mice show a transient tail spike ~10 min into rotation.
398 When nausea or dizziness is present, the head temperature drop takes longer to recover, and
399 the transient tail spike diminishes or disappears. **B,C,D.** Viral infection diminishes tail
400 vasodilatations and impairs a mouse's natural response to the provocative motion. At time t = 0,
401 mice experience a 20-minute provocative motion and exhibit a significant increase in tail
402 temperature. Δ tails are computed and are corrected for ambient temperature. Findings suggest
403 that olcegepant did not protect against virus-induced changes in tail vasodilation at 3 dpi in all of
404 the strains tested. **E,F,G.** Viral infection impacts recovery from hypothermia after provocative
405 motion. **H.** Second order curve fits observed recovery of head temperatures after provocative
406 motion to baseline. Across all strains, mice experienced delayed temperature recovery
407 compared to pretest, with longer recovery profiles. **I.** No protective effects were seen by
408 olcegepant in temperature recovery for any of the tested strains.

409

410

411 **Fig. 4.** Bronco-alveolar lavage (BAL) samples were obtained for ELISA testing, and lungs were
412 obtained for subsequent immunohistochemistry at 3 dpi. MA-SARS-CoV-2 infection increased
413 the release of the inflammatory cytokine IL-6, and this IL-6 release was attenuated by CGRP
414 signaling blockade. In both C57B6/J **(A)** and 129S mice **(B)** strains, IL-6 release was

415 attenuated by olcegepant SQ release. Moreover, in αCGRP null mice, IL-6 cytokine release was
416 statistically equivalent to non-infected controls **(B)**.
417
418 **Fig. 5.** Older (18 months) female and male mice were tested for weight loss and core
419 temperature drops after infection with MA-10 SARS-CoV-2, 10^5 pfu virus at 0-7 dpi. **A. C.** We
420 found that animals treated with olcegepant recovered from the initial weight loss, with male mice
421 showing increased protection. **A.** C57B6/J; **C.** 129S. **E.** Similar to the IL-6 findings (**Fig. 4**),
422 mice lacking the CGRP peptide were not significantly different from uninfected controls. **B, D,**
423 **F.** Viral infection caused core temperatures of mice to decrease, and this effect was unaltered
424 by olcegepant treatment.
425
426 **Fig. 6.** A**&B.** There was no statistically significant difference in the number of SARS-CoV-2
427 antigen-positive cells in the lungs of (**A, C**) C57/B6J or (**B, D**) 129 mice, between mice that
428 received placebo versus olcegepant pellets at 3 dpi. **C, D.** Representative SARS-CoV-2
429 immunostaining is shown for 3 dpi lung issues from C57B6/J (**C**), and 129S (**D**) mice. Scale bar
430 is 100 μm. (*= $p < 0.05$, ** =$p < 0.01$, ** *= $p < 0.001$, **** = $p < 0.0001$)
431

432 **References:**

433 Abobaker, A., and M. Darrat. 2021. 'Letter to the Editor From Abobaker and Darrat: "Circulating
434 Levels of Calcitonin Gene-Related Peptide Are Lower in COVID-19 Patients"', *J Endocr*
435 *Soc*, 5: bvab052.

436 Achanta, R., A. Shaji, K. Smith, A. Lucchi, P. Fua, and S. Susstrunk. 2012. 'SLIC superpixels
437 compared to state-of-the-art superpixel methods', *IEEE Trans Pattern Anal Mach Intell*,
438 34: 2274-82.

439 Aedo-Sanchez, C., G. Gutierrez, and E. Aguilar-Vidal. 2023. 'COVID-19 and Vestibular
440 Symptoms and Assessment: A Review', *Audiol Neurootol*: 1-7.

441 Aghagoli, G., B. Gallo Marin, N. J. Katchur, F. Chaves-Sell, W. F. Asaad, and S. A. Murphy.
442 2021. 'Neurological Involvement in COVID-19 and Potential Mechanisms: A Review',
443 *Neurocrit Care*, 34: 1062-71.

444 Assas, B. M., J. A. Miyan, and J. L. Pennock. 2014. 'Cross-talk between neural and immune
445 receptors provides a potential mechanism of homeostatic regulation in the gut mucosa',
446 *Mucosal Immunol*, 7: 1283-9.

447 Assas, B. M., J. I. Pennock, and J. A. Miyan. 2014. 'Calcitonin gene-related peptide is a key
448 neurotransmitter in the neuro-immune axis', *Front Neurosci*, 8: 23.

449 Bankhead, P., M. B. Loughrey, J. A. Fernandez, Y. Dombrowski, D. G. McArt, P. D. Dunne, S.
450 McQuaid, R. T. Gray, L. J. Murray, H. G. Coleman, J. A. James, M. Salto-Tellez, and P.
451 W. Hamilton. 2017. 'QuPath: Open source software for digital pathology image analysis',
452 *Sci Rep*, 7: 16878.

453 Bohn, M. K., A. Hall, L. Sepiashvili, B. Jung, S. Steele, and K. Adeli. 2020. 'Pathophysiology of
454 COVID-19: Mechanisms Underlying Disease Severity and Progression', *Physiology*
455 *(Bethesda)*, 35: 288-301.

456 Bolay, H., O. Karadas, B. Ozturk, R. Sonkaya, B. Tasdelen, T. D. S. Bulut, O. Gulbahar, A.
457 Ozge, and B. Baykan. 2021. 'HMGB1, NLRP3, IL-6 and ACE2 levels are elevated in
458 COVID-19 with headache: a window to the infection-related headache mechanism', *J*
459 *Headache Pain*, 22: 94.

460 Caronna, E., V. Jose Gallardo, A. Alpuente, M. Torres-Ferrus, N. M. Sanchez-Mateo, J.
461 Viguera-Romero, A. C. Lopez-Veloso, A. Lopez-Bravo, A. B. Gago-Veiga, P. Irimia
462 Sieira, J. Porta-Etessam, S. Santos-Lasaosa, P. Pozo-Rosich, and Cgrp-Covid Study
463 Group Spanish. 2021. 'Safety of anti-CGRP monoclonal antibodies in patients with
464 migraine during the COVID-19 pandemic: Present and future implications', *Neurologia*
465 *(Engl Ed)*, 36: 611-17.

466 Carpenter, K. C., J. Yang, and J. J. Xu. 2023. 'Animal Models for the Study of Neurologic
467 Manifestations Of COVID-19', *Comp Med*, 73: 91-103.

468 Channappanavar, R., and S. Perlman. 2017. 'Pathogenic human coronavirus infections: causes
469 and consequences of cytokine storm and immunopathology', *Semin Immunopathol*, 39:
470 529-39.

471 Del Vecchio, F., E. Nalivaiko, M. Cerri, M. Luppi, and R. Amici. 2014. 'Provocative motion
472 causes fall in brain temperature and affects sleep in rats', *Exp Brain Res*, 232: 2591-9.

473 Dinnon, K. H., 3rd, S. R. Leist, A. Schafer, C. E. Edwards, D. R. Martinez, S. A. Montgomery, A.
474 West, B. L. Yount, Jr., Y. J. Hou, L. E. Adams, K. L. Gully, A. J. Brown, E. Huang, M. D.
475 Bryant, I. C. Choong, J. S. Glenn, L. E. Gralinski, T. P. Sheahan, and R. S. Baric. 2020.

476 'A mouse-adapted model of SARS-CoV-2 to test COVID-19 countermeasures', *Nature*,
477 586: 560-66.

478 ———. 2021. 'Publisher Correction: A mouse-adapted model of SARS-CoV-2 to test COVID-19
479 countermeasures', *Nature*, 590: E22.

480 Dinnon, K. H., S. R. Leist, K. Okuda, H. Dang, E. J. Fritch, K. L. Gully, G. De la Cruz, M. D.
481 Evangelista, T. Asakura, R. C. Gilmore, P. Hawkins, S. Nakano, A. West, A. Schafer, L.
482 E. Gralinski, J. L. Everman, S. P. Sajuthi, M. R. Zweigart, S. Dong, J. McBride, M. R.
483 Cooley, J. B. Hines, M. K. Love, S. D. Groshong, A. VanSchoiack, S. J. Phelan, Y.
484 Liang, T. Hether, M. Leon, R. E. Zumwalt, L. M. Barton, E. J. Duval, S. Mukhopadhyay,
485 E. Stroberg, A. Borczuk, L. B. Thorne, M. K. Sakthivel, Y. Z. Lee, J. S. Hagood, J. R.
486 Mock, M. A. Seibold, W. K. O'Neal, S. A. Montgomery, R. C. Boucher, and R. S. Baric.
487 2022. 'A model of persistent post SARS-CoV-2 induced lung disease for target
488 identification and testing of therapeutic strategies', *bioRxiv*.

489 Doods, H., G. Hallermayer, D. Wu, M. Entzeroth, K. Rudolf, W. Engel, and W. Eberlein. 2000.
490 'Pharmacological profile of BIBN4096BS, the first selective small molecule CGRP
491 antagonist', *Br J Pharmacol*, 129: 420-3.

492 Doyle, M. F. 2022. 'Central nervous system outcomes of COVID-19', *Transl Res*, 241: 41-51.

493 Grassini, A., A. Marcinno, F. Roveta, E. Gallo, A. Cermelli, S. Boschi, E. Rubino, and I. Rainero.
494 2021. 'Impact of COVID-19 on chronic migraine treated with erenumab: a case report',
495 *Neurol Sci*, 42: 3079-81.

496 Han, D. 2019. 'Association of Serum Levels of Calcitonin Gene-related Peptide and Cytokines
497 during Migraine Attacks', *Ann Indian Acad Neurol*, 22: 277-81.

498 Jeong, M., K. E. Ocwieja, D. Han, P. A. Wackym, Y. Zhang, A. Brown, C. Moncada, A.
499 Vambutas, T. Kanne, R. Crain, N. Siegel, V. Leger, F. Santos, D. B. Welling, L. Gehrke,
500 and K. M. Stankovic. 2021. 'Direct SARS-CoV-2 infection of the human inner ear may
501 underlie COVID-19-associated audiovestibular dysfunction', *Commun Med (Lond)*, 1: 44.

502 Karadas, O., B. Ozturk, A. R. Sonkaya, B. Tasdelen, A. Ozge, and H. Bolay. 2021. 'Latent class
503 cluster analysis identified hidden headache phenotypes in COVID-19: impact of
504 pulmonary infiltration and IL-6', *Neurol Sci*, 42: 1665-73.

505 Kuba, K., Y. Imai, S. Rao, H. Gao, F. Guo, B. Guan, Y. Huan, P. Yang, Y. Zhang, W. Deng, L.
506 Bao, B. Zhang, G. Liu, Z. Wang, M. Chappell, Y. Liu, D. Zheng, A. Leibbrandt, T. Wada,
507 A. S. Slutsky, D. Liu, C. Qin, C. Jiang, and J. M. Penninger. 2005. 'A crucial role of
508 angiotensin converting enzyme 2 (ACE2) in SARS coronavirus-induced lung injury', *Nat*
509 *Med*, 11: 875-9.

510 Littlefield, K. M., R. O. Watson, J. M. Schneider, C. P. Neff, E. Yamada, M. Zhang, T. B.
511 Campbell, M. T. Falta, S. E. Jolley, A. P. Fontenot, and B. E. Palmer. 2022. 'SARS-CoV-
512 2-specific T cells associate with inflammation and reduced lung function in pulmonary
513 post-acute sequalae of SARS-CoV-2', *PLoS Pathog*, 18: e1010359.

514 Liu, Y., C. Zhang, F. Huang, Y. Yang, F. Wang, J. Yuan, Z. Zhang, Y. Qin, X. Li, D. Zhao, S. Li,
515 S. Tan, Z. Wang, J. Li, C. Shen, J. Li, L. Peng, W. Wu, M. Cao, L. Xing, Z. Xu, L. Chen,
516 C. Zhou, W. J. Liu, L. Liu, and C. Jiang. 2020. 'Elevated plasma levels of selective
517 cytokines in COVID-19 patients reflect viral load and lung injury', *Natl Sci Rev*, 7: 1003-
518 11.

519 Mallee, J. J., C. A. Salvatore, B. LeBourdelles, K. R. Oliver, J. Longmore, K. S. Koblan, and S.
520 A. Kane. 2002. 'Receptor activity-modifying protein 1 determines the species selectivity
521 of non-peptide CGRP receptor antagonists', *J Biol Chem*, 277: 14294-8.

522 Mazloumi Gavgani, A., D. M. Hodgson, and E. Nalivaiko. 2017. 'Effects of visual flow direction
523 on signs and symptoms of cybersickness', *PLoS One*, 12: e0182790.

524 Ngampramuan, S., M. Cerri, F. Del Vecchio, J. J. Corrigan, A. Kamphee, A. S. Dragic, J. A.
525 Rudd, A. A. Romanovsky, and E. Nalivaiko. 2014. 'Thermoregulatory correlates of
526 nausea in rats and musk shrews', *Oncotarget*, 5: 1565-75.

527 Ochoa-Callejero, L., J. Garcia-Sanmartin, P. Villoslada-Blanco, M. Iniguez, P. Perez-Matute, E.
528 Pujadas, R. Brody, J. A. Oteo, and A. Martinez. 2021. 'Response to Letter to the Editor
529 from Abobaker and Darrat: "Circulating levels of Calcitonin Gene-Related Peptide Are
530 Lower in COVID-19 Patients"', *J Endocr Soc*, 5: bvab053.

531 Ozkan, E., O. Celebi, O. Keskin, A. Gursoy, and Y. Gursoy-Ozdemir. 2022. 'Is Persistent Post-
532 COVID Headache Associated With Protein-Protein Interactions Between Antibodies
533 Against Viral Spike Protein and CGRP Receptor?: A Case Report', *Front Pain Res*
534 *(Lausanne)*, 3: 858709.

535 Rizzi, M., S. Tonello, F. Morani, E. Rizzi, G. F. Casciaro, E. Matino, M. Costanzo, E. Zecca, A.
536 Croce, A. Pedrinelli, V. Vassia, R. Landi, V. R. Mallela, D. D'Onghia, R. Minisini, M.
537 Bellan, L. M. Castello, F. Gavelli, G. C. Avanzi, F. Patrucco, M. Pirisi, D. Colangelo, and
538 P. P. Sainaghi. 2022. 'CGRP Plasma Levels Correlate with the Clinical Evolution and
539 Prognosis of Hospitalized Acute COVID-19 Patients', *Viruses*, 14.

540 Robertson, C. E. 2020. 'Could CGRP antagonists be helpful in the fight against COVID-19?',
541 *Headache*.

542 Romano, F., N. Caramia, D. Straumann, E. Nalivaiko, and G. Bertolini. 2017. 'Cross-coupling
543 vestibular stimulation: motion sickness and the vestibulo-sympathetic reflex', *J Neurol*.

544 Saniasiaya, J., and J. Kulasegarah. 2021. 'Dizziness and COVID-19', *Ear Nose Throat J*, 100:
545 29-30.

546 Shapira, T., I. A. Monreal, S. P. Dion, D. W. Buchholz, B. Imbiakha, A. D. Olmstead, M. Jager,
547 A. Desilets, G. Gao, M. Martins, T. Vandal, C. A. H. Thompson, A. Chin, W. D. Rees, T.
548 Steiner, I. R. Nabi, E. Marsault, J. Sahler, D. G. Diel, G. R. Van de Walle, A. August, G.
549 R. Whittaker, P. L. Boudreault, R. Leduc, H. C. Aguilar, and F. Jean. 2022. 'A TMPRSS2
550 inhibitor acts as a pan-SARS-CoV-2 prophylactic and therapeutic', *Nature*, 605: 340-48.

551 Shapira, T., I. A. Monreal, S. P. Dion, M. Jager, A. Desilets, A. D. Olmstead, T. Vandal, D. W.
552 Buchholz, B. Imbiakha, G. Gao, A. Chin, W. D. Rees, T. Steiner, I. R. Nabi, E. Marsault,
553 J. Sahler, A. August, G. Van de Walle, G. R. Whittaker, P. L. Boudreault, H. C. Aguilar,
554 R. Leduc, and F. Jean. 2021. 'A novel highly potent inhibitor of TMPRSS2-like proteases
555 blocks SARS-CoV-2 variants of concern and is broadly protective against infection and
556 mortality in mice', *bioRxiv*.

557 Tu, L., L. Poppi, J. Rudd, E. T. Cresswell, D. W. Smith, A. Brichta, and E. Nalivaiko. 2017.
558 'Alpha-9 nicotinic acetylcholine receptors mediate hypothermic responses elicited by
559 provocative motion in mice', *Physiol Behav*, 174: 114-19.

560 Zhu, N., D. Zhang, W. Wang, X. Li, B. Yang, J. Song, X. Zhao, B. Huang, W. Shi, R. Lu, P. Niu,
561 F. Zhan, X. Ma, D. Wang, W. Xu, G. Wu, G. F. Gao, W. Tan, Investigating China Novel
562 Coronavirus, and Team Research. 2020. 'A Novel Coronavirus from Patients with
563 Pneumonia in China, 2019', *N Engl J Med*, 382: 727-33.

564 Ziegler, C. G. K., S. J. Allon, S. K. Nyquist, I. M. Mbano, V. N. Miao, C. N. Tzouanas, Y. Cao, A.
565 S. Yousif, J. Bals, B. M. Hauser, J. Feldman, C. Muus, M. H. Wadsworth, 2nd, S. W.
566 Kazer, T. K. Hughes, B. Doran, G. J. Gatter, M. Vukovic, F. Taliaferro, B. E. Mead, Z.
567 Guo, J. P. Wang, D. Gras, M. Plaisant, M. Ansari, I. Angelidis, H. Adler, J. M. S. Sucre,

568 C. J. Taylor, B. Lin, A. Waghray, V. Mitsialis, D. F. Dwyer, K. M. Buchheit, J. A. Boyce,
569 N. A. Barrett, T. M. Laidlaw, S. L. Carroll, L. Colonna, V. Tkachev, C. W. Peterson, A.
570 Yu, H. B. Zheng, H. P. Gideon, C. G. Winchell, P. L. Lin, C. D. Bingle, S. B. Snapper, J.
571 A. Kropski, F. J. Theis, H. B. Schiller, L. E. Zaragosi, P. Barbry, A. Leslie, H. P. Kiem, J.
572 L. Flynn, S. M. Fortune, B. Berger, R. W. Finberg, L. S. Kean, M. Garber, A. G. Schmidt,
573 D. Lingwood, A. K. Shalek, J. Ordovas-Montanes, H. C. A. Lung Biological Network.
574 Electronic address: lung-network@humancellatlas.org, and H. C. A. Lung Biological
575 Network. 2020. 'SARS-CoV-2 Receptor ACE2 Is an Interferon-Stimulated Gene in
576 Human Airway Epithelial Cells and Is Detected in Specific Cell Subsets across Tissues',
577 *Cell*.
578